

# Supplementary Information for

## Shape and stiffness memory ionogels with programmable pressure-resistance response

Shuyun Zhuo<sup>1</sup>, Cheng Song<sup>1</sup>, Qinfeng Rong<sup>2</sup>, Tianyi Zhao<sup>1\*</sup> and Mingjie Liu<sup>1,3,4,5\*</sup>

\*Corresponding author. Email: zhaoty@buaa.edu.cn, liumj@buaa.edu.cn

### **This PDF file includes:**

- Supplementary Note 1. Characterization of microstructure.
- Supplementary Note 2. Differential scanning calorimeter (DSC) measurements.
- Supplementary Note 3. Measurements of rheological properties.
- Supplementary Note 4. Measurements of shape memory properties.
- Supplementary Note 5. Measurements of mechanical properties.
- Supplementary Note 6. Measurements of self-recovery capacity.
- Supplementary Note 7. Measurements of pressure-resistance performance of the ionogel pressure sensor.
- Supplementary Figure 1. Structure characterization of the heterophasic ionogels.
- Supplementary Figure 2. Shape memory property of the heterophasic ionogels.
- Supplementary Figure 3. POM images of the ionogel framework.
- Supplementary Figure 4. Strain-stress curves of the heterophasic ionogel and ionogel framework.
- Supplementary Figure 5. Strain-stress curves of the heterophasic ionogels.
- Supplementary Figure 6. Switchable mechanics of the heterophasic ionogels.
- Supplementary Figure 7. Weight and structure changes of the heterophasic ionogels.
- Supplementary Figure 8. Resistance change of the ionogel sensors.
- Supplementary Figure 9. Resistance changes of the ionogel sensors under different strain and pressure.
- Supplementary Figure 10. Resistance changes of the ionogel sensors in monitoring physiological signals.
- Supplementary Figure 11. The cyclic loading-unloading compressive tests of the heterophasic ionogels.
- Supplementary Figure 12. The cyclic loading-unloading compressive tests of original ionic gels.
- Supplementary Figure 13. The cyclic loading-unloading compressive tests of recovered ionogels.

30 Supplementary Figure 14. The durable strain-sensitive test.

31 Supplementary Figure 15. Resistance response of the ionogel sensors under various pressure.

### 32 **Supplementary Note 1. Characterization of microstructure**

33 The oil-in-IL emulsion was characterized using an optical microscope (Nikon LV100N).  
34 Polarized optical microscope (Leica DC 300) was used to observe the isotropic and anisotropic  
35 structure of the ionogels. The microstructures of the heterophasic ionogel samples were  
36 characterized using a scanning electron microscopy (SEM, JEOL-7500 apparatus, at an  
37 accelerating voltage of 5 kV) and a confocal laser scanning microscopy (CLSM, Olympus  
38 FV1000-IX81 confocal laser biological microscope). For CLSM measurements, the IL-gels were  
39 stained with the hydrophilic dyes (DAPI, blue), and the microorganogel domains were stained with  
40 the oleophilic dyes (Perylene Red, red).

### 41 **Supplementary Note 2. Differential scanning calorimeter (DSC) measurements**

42 DSC measurements were conducted on the PerkinElmer Pyris 1 TGA under nitrogen  
43 atmosphere. The original heterophasic ionogel samples, P(AA-VBIMBF<sub>4</sub>), and EMIMBF<sub>4</sub>, sealed  
44 in aluminum pans, were scanned between -150 and 100°C at a scanning rate of 10 °C/min.

### 45 **Supplementary Note 3. Measurements of rheological properties**

46 The rheological properties of the original heterophasic ionogel samples were investigated on  
47 an Anton Paar model MCR-301 rheometer. The heterophasic ionogel samples in form of sheets  
48 (15 mm diameter × 2 mm height) were set under a 15 mm diameter parallel plate. Under a variety  
49 of temperatures, the storage moduli ( $G'$ ) of the heterophasic ionogels were swept at 15.8 rad s<sup>-1</sup>  
50 and a constant strain ( $\gamma$ ) of 0.1 %. In cyclic tests, the storage moduli were repeatedly measured  
51 through heating-cooling the original ionogel samples (0 and 50 °C).

### 52 **Supplementary Note 4. Measurements of shape memory properties**

53 Compressing/recovering test was conducted on cylinder-shaped (6 mm diameter × 5 mm  
54 height) ionogel samples to evaluate shape memory effect. The samples were compressed by 70%

55 at 45 °C and cooled at 5 °C for 5 min with compression force on. Then the external force was  
56 removed to record the height of the fixed samples. With temperature increasing and remaining  
57 45 °C for 5min, the samples recovered. Shape fixity ( $R_f$ ) and shape recovery ( $R_r$ ) were calculated  
58 to indicate the shape memory property.  $R_f = 100\% \times (h_0 - h_f) / (70\% h_0)$ ,  $R_r = 100\% \times (h_r - h_f) / (h_0 - h_f)$ ,  
59 where  $h_0$ ,  $h_f$ ,  $h_r$  represent the original height, fixed height, and recovered height.

#### 60 **Supplementary Note 5. Measurements of mechanical properties**

61 The compression and tensile measurements of heterophasic ionogels at varying temperatures  
62 were performed using a tensile-compressive tester with a 1000 N load cell (Tensilon HZ-1004D,  
63 Hengzhun Instrument Technology Co., China). In tensile test, cylinder-shaped (6 mm diameter ×  
64 30 mm height) original samples were stretched at a strain rate of 10 mm min<sup>-1</sup> up to a maximum  
65 strain  $\epsilon_m$ . In compression tests, cylinder-shaped (6 mm diameter × 5 mm height) original and  
66 compressed samples were measured at a constant compression rate of 10 mm min<sup>-1</sup>. The modulus  
67 was calculated from the linear slope of the stress-strain curves between 0-10 % compression.

#### 68 **Supplementary Note 6. Measurements of self-recovery capacity**

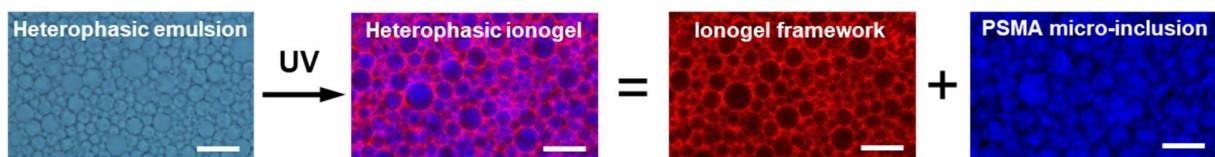
69 Cyclic loading-unloading test was carried out to evaluated self-recoverable property of the  
70 original heterophasic ionogels. The cylinder-shaped (6 mm diameter × 5 mm height) original  
71 samples were compressed by 70% at a constant loading/unloading rate of 10 mm min<sup>-1</sup>. Then these  
72 samples were heated to 45 °C for 2 hours and cooled at 5 °C for 2 hours. At last, the self-recovered  
73 samples were tested again to show the recovery capability of the heterophasic ionogels.

#### 74 **Supplementary Note 7. Measurements of pressure-resistance performance of the ionogel** 75 **pressure sensor**

76 Resistance changes was recorded by a HIOKI IM3536 LCR meter. The prepared pressure  
77 sensors were precisely compressed and released in a controlled manner using a tensile-

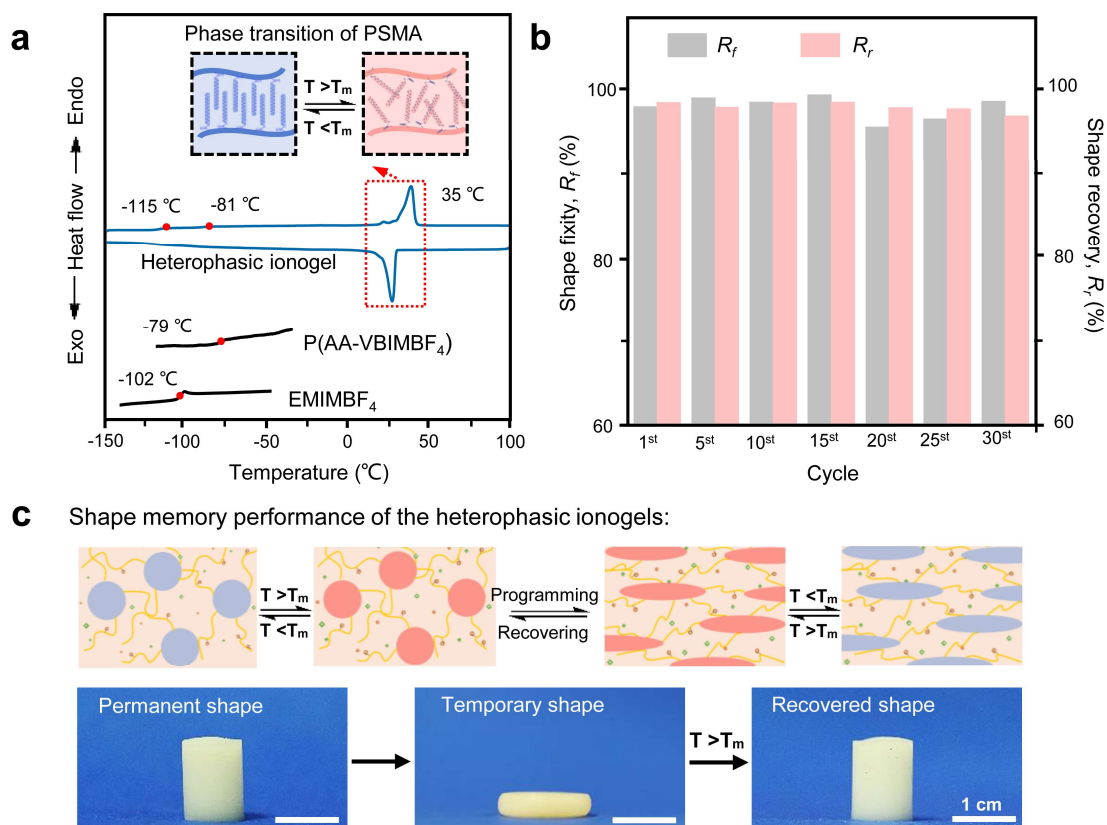
78 compressive tester with a 100 N load cell (Tensilon HZ-1004D, Hengzhun Instrument Technology  
79 Co., China) and a computer-controlled force gauge (ESM301 from Mark-10 Corporation). All of  
80 the pressure-resistance tests were conducted in an ambient environment, and the compression rate  
81 was set at 20 mm min<sup>-1</sup>. In the human motions test, the sensors were fixed under the shoe sole. To  
82 test the detection limit of the pressure sensors, we use a computer-controlled force gauge to apply  
83 a stepped pressure of 0.01 N to the sensors until obvious and repeatable resistance change appeared.  
84 To ensure the accuracy, every test was repeated three times using different samples.

85  
86  
87  
88  
89  
90  
91  
92



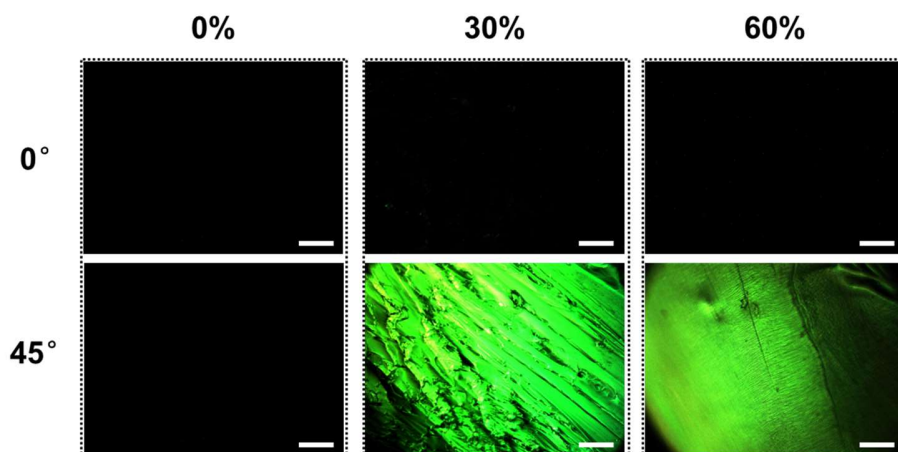
93  
94 **Supplementary Figure 1.** Optical image of the heterophasic emulsion and confocal laser scanning  
95 microscopy image of the heterophasic ionogels with red-stained ionogel framework and blue-  
96 stained PSMA micro-inclusions. Scale bar, 10  $\mu\text{m}$ .

97  
98



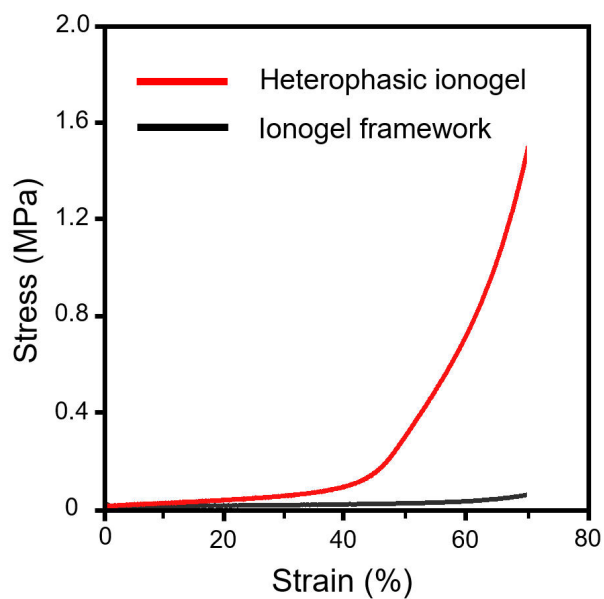
99  
 100 **Supplementary Figure 2. Shape memory property of the heterophasic ionogels. (a)**  
 101 **Differential scanning calorimetry (DSC) curves of the heterophasic ionogel and components:**  
 102 **P(AA-VBIMBF<sub>4</sub>) and EMIMBF<sub>4</sub>. Illustration shows the phase transition of PSMA micro-**  
 103 **inclusions. (b) Shape fixity ( $R_f$ ) and shape recovery ( $R_r$ ) of the heterophasic ionogels at different**  
 104 **shape memory cycles. (c) shape memory performance of the heterophasic ionogels, scale bar, 1**  
 105 **cm.**

106



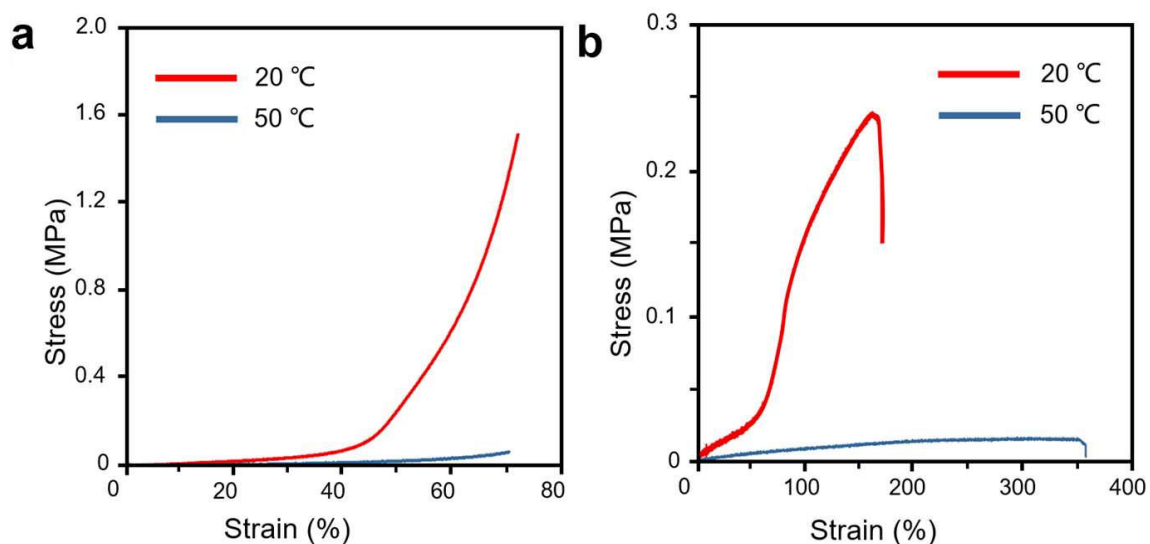
107  
108  
109  
110  
111  
112

**Supplementary Figure 3.** POM images of the ionogel framework at different compression ratio, scale bar, 200  $\mu\text{m}$ .



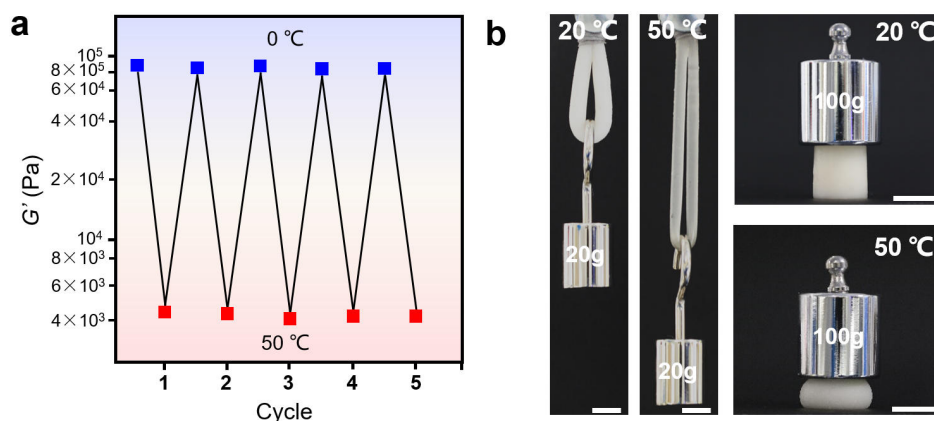
113  
114  
115  
116  
117  
118

**Supplementary Figure 4.** Strain-stress curves of the original heterophasic ionogel and ionogel framework.



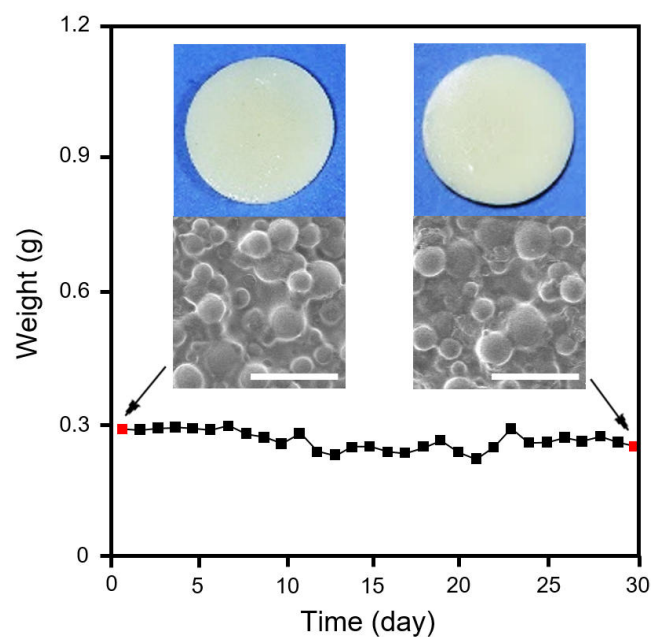
119  
 120 **Supplementary Figure 5.** Strain-stress curves of the original heterophasic ionogels under (a)  
 121 compression and (b) stretching at different temperatures.

122  
 123



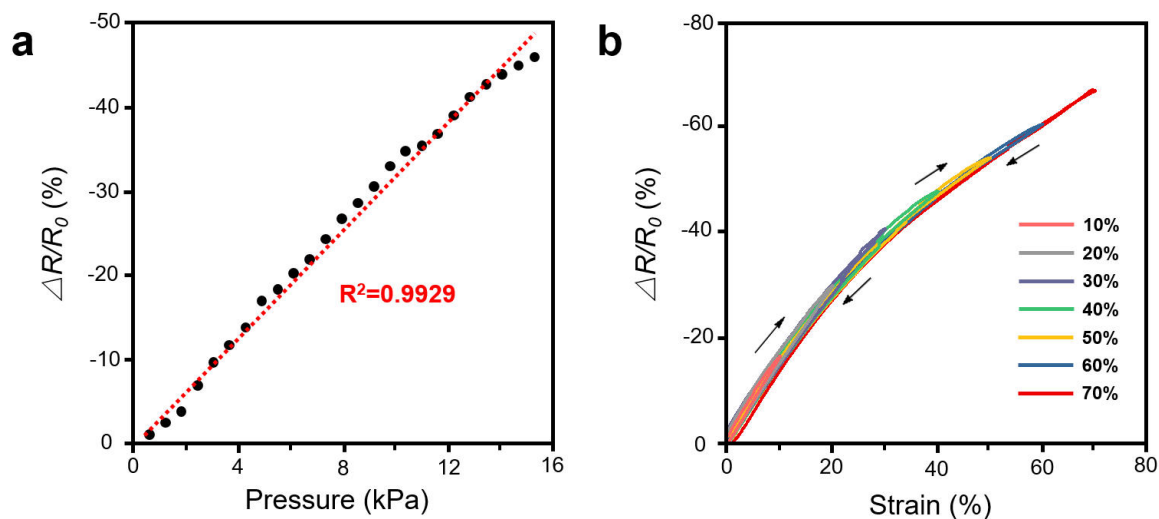
124  
 125 **Supplementary Figure 6.** Switchable mechanics of the original heterophasic ionogels. (a)  
 126 Reversibly switched modulus of the heterophasic ionogel at 0 °C and 50 °C. (b) Pictures showing  
 127 the heterophasic ionogels with low stretching/compression ratio at 20 °C and high at 50 °C. Scale  
 128 bar, 1 cm.

129  
 130



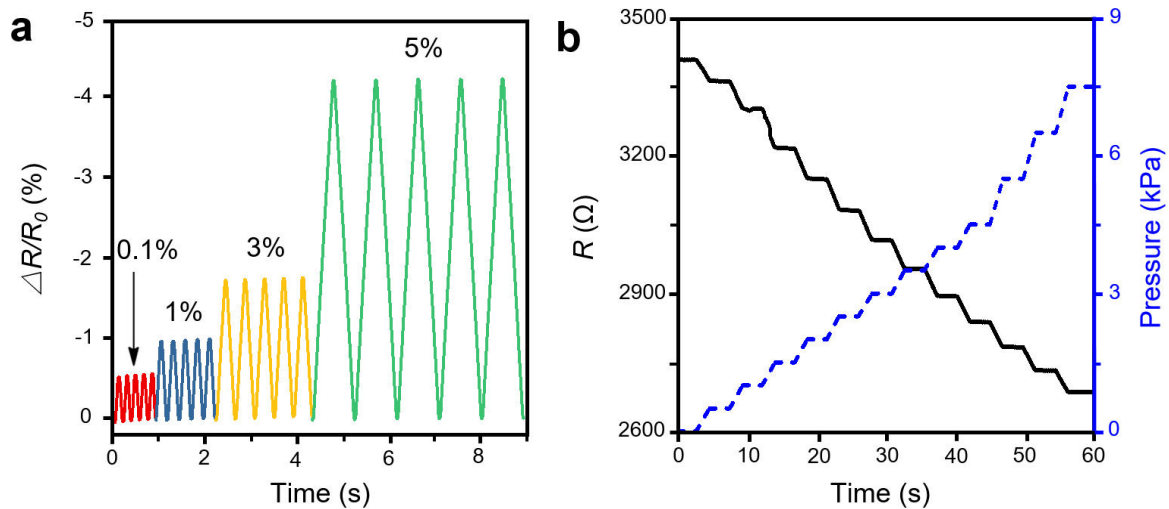
131  
 132 **Supplementary Figure 7.** Weight and structure changes during exposure in the air for 30 d  
 133 revealing good stability of the original heterophasic ionogels. Scale bar, 10 $\mu$ m.

134  
 135  
 136



137  
 138 **Supplementary Figure 8.** Resistance change of the original ionogel sensors: (a) in pressure  
 139 range of 0-16 kPa, (b) during compressing/releasing cycles.

140  
 141  
 142  
 143



144

145 **Supplementary Figure 9.** Resistance changes of the original ionogel-based sensors under

146 different strain (a) and pressure (b).

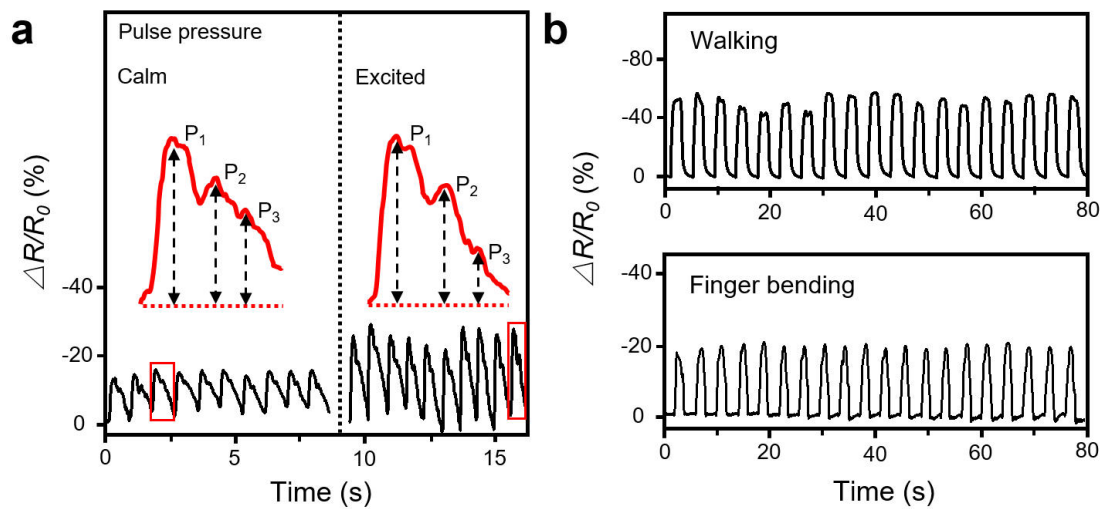
147

148

149

150

151



152

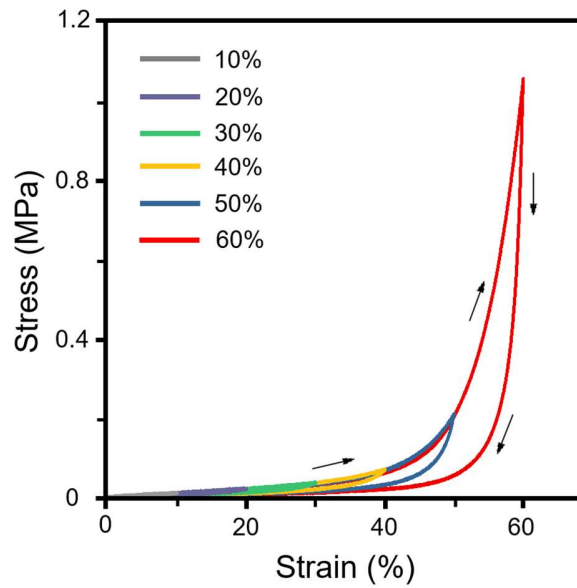
153 **Supplementary Figure 10.** Sensing ability of the original ionogel-based sensors. (a) Real-

154 time pulse signals monitored by the ionogel sensor. The expanded pulse wave contains three

155 peaks. (b) Response of the ionogel sensors in monitoring human motion (walking and finger

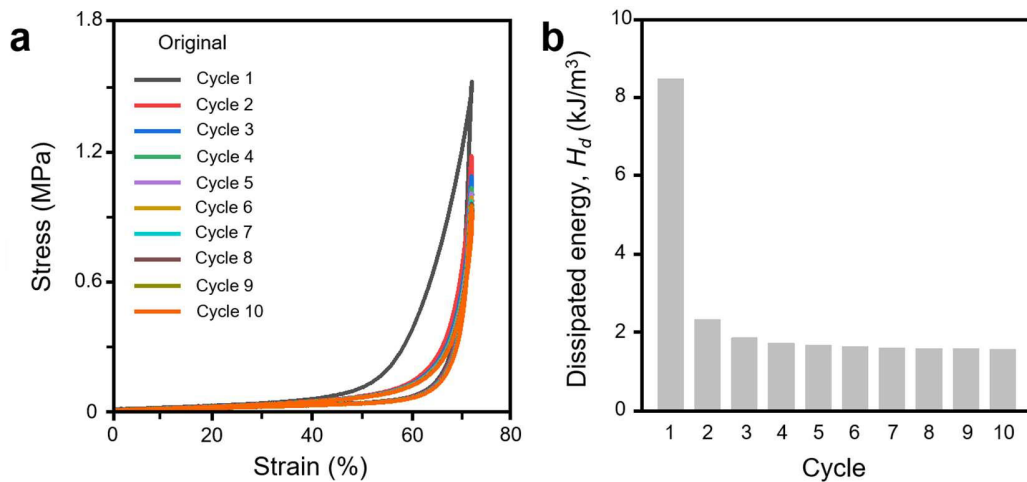
156 bending).

157



158  
 159 **Supplementary Figure 11.** The cyclic loading-unloading compressive tests of the original  
 160 heterophasic ionogels with different compressive strains at 20 °C.

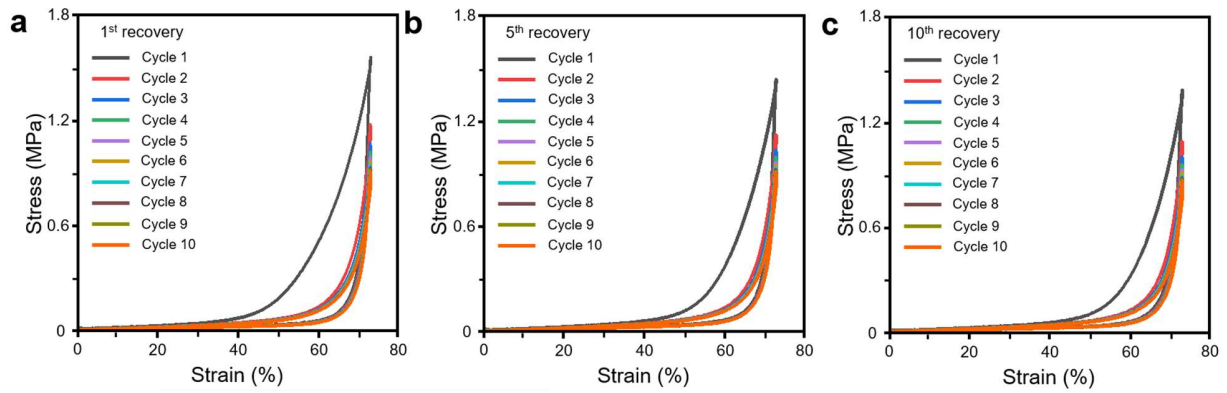
161  
 162  
 163



164  
 165 **Supplementary Figure 12.** The cyclic loading-unloading compressive tests of original  
 166 **ionogels.** (a) Strain-stress curves during the cycle 1-10; (b) Dissipated energy of the original  
 167 heterophasic ionogels at different loading-unloading cycles.

168  
 169

170  
171  
172



173

174

**Supplementary Figure 13. The cyclic loading-unloading compressive tests of recovered**

175

**ionogels: (a) 1<sup>st</sup> recovery; (b) 5<sup>th</sup> recovery and (c) 10<sup>th</sup> recovery.**

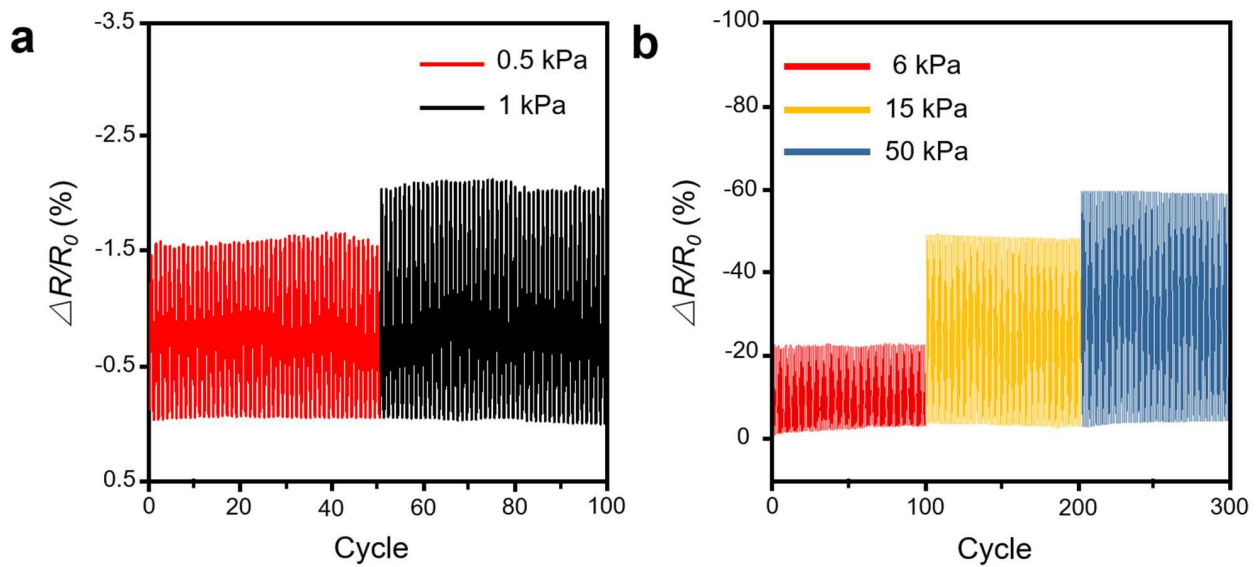
176

177

178

179

180



181

182

**Supplementary Figure 14. The durable strain-sensitive test at (a) low pressure and (b) high**

183

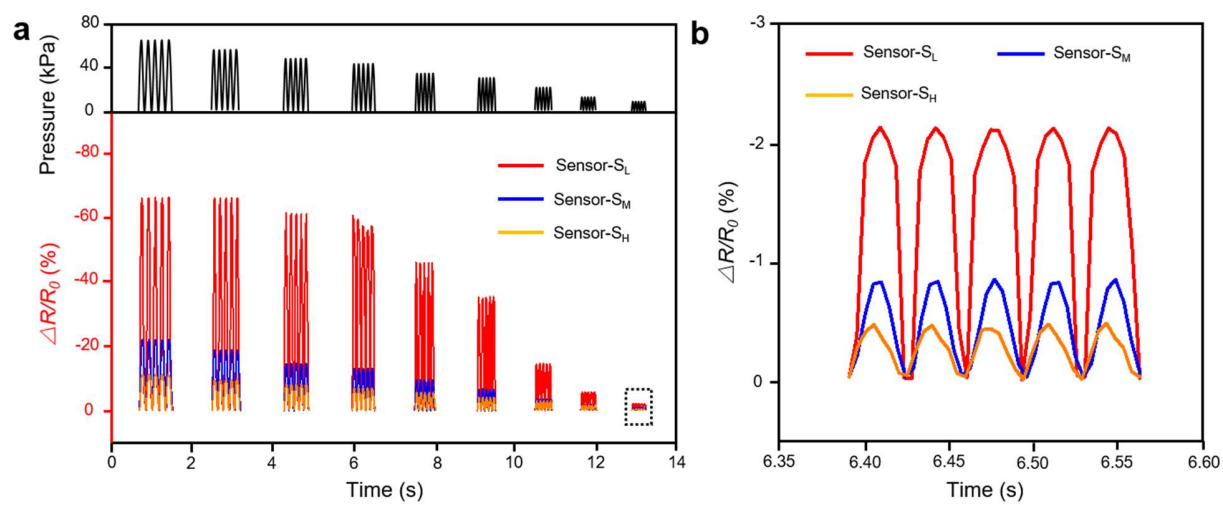
**pressure.**

184

185

186

187  
188



189  
190

**Supplementary Figure 15.** Resistance response of the ionogel sensors under various pressure.